Magnetic phase diagram of $NiCl_2 \cdot 4H_2O$

C. C. Becerra, N. F. Oliveira Jr., and A. Paduan-Filho
Instituto de Física da Universidade de São Paulo, Caixa Postal 20516, CEP 01498, São Paulo, São Paulo, Brazil

W. Figueiredo and M. V. P. Souza
Departamento de Física da Universidade Federal de Santa Catarina, Florianópolis, Santa Catarina, Brazil
(Received 21 September 1987; revised manuscript received 12 May 1988)

The magnetic phase diagrams of the monoclinic antiferromagnet $NiCl_2 \cdot 4H_2O$ were determined from differential susceptibility measurements, for external fields applied along the easy axis (c), and along the two principal perpendicular directions (b and a'). The Néel temperature is $T_N = 3.00 \pm 0.01$ K. The $T=0$ transition fields are $H_c(0) = 68.35$ kOe, $H_b(0) = 77.54$ kOe, $H_{a'}(0) = 86.40$ kOe, and $H_{SF}(0) = 23.0$ kOe for the spin-flop transition. These fields were used to determine the parameters of a spin Hamiltonian that included anisotropic exchange and orthorhombic single-ion anisotropy. The results show a slightly anisotropic exchange and a strong crystalline-field anisotropy in the plane perpendicular to the easy axis. Several aspects of the phase diagrams are discussed and found to be consistent with such a spin Hamiltonian. In particular, spin-wave calculations of the low-T paramagnetic boundaries yielded results that agreed with the data not only in the predicted T^2 dependence, but also in the coefficients of the T^2.

I. INTRODUCTION

The experimental determination of the magnetic field ($\mathbf{H}$) versus temperature (T) phase boundaries of low-anisotropy antiferromagnets[1] is of interest for several reasons. First, the $T=0$ transition fields, obtained from extrapolations of the low-T boundaries, provide a direct evaluation of the phenomenological exchange and anisotropy parameters. Second, various theoretical predictions for the temperature dependence of the transition fields can be compared with the experimental data. In this paper we present the magnetic phase diagrams of $NiCl_2 \cdot 4H_2O$ determined from differential magnetization measurements, for $\mathbf{H}$ along the three principal magnetic axes. The data are shown to be campatible with an orthorhombic single-ion Hamiltonian. Using this Hamiltonian we calculate the low-T paramagnetic boundaries with a spin-wave approach and find the predicted boundaries to be consistent with the experimental ones. We also discuss the existent theoretical predictions for the Néel temperature, T_N, and for the region near the bicritical point, and compare them with the experimental data.

Zero-field susceptibility and specific heat of $NiCl_2 \cdot 4H_2O$ were measured by McElearney *et al.*[2] Their interpretation of the data led to an exchange parameter too high when compared with T_N, and anisotropy parameters of practically uniaxial symmetry (the orthorhombic parameter was practically zero). These results were contested in a short communication,[3] in which part of the present easy-axis data were presented, showing that their parameters were totally incompatible with our easy-axis $T=0$ transition fields. In that communication, better estimates of the exchange and anisotropy fields were given, still in a simplified model of isotropic exchange and uniaxial symmetry because this was all the data allowed. In the present work, the addition of boundaries for $\mathbf{H}$ perpendicular to the easy-axis has made it possible to examine a more complete model Hamiltonian in which anisotropic exchange as well as orthorhombic single-ion anisotropy was included. The set of parameters obtained show a slightly anisotropic exchange and a single-ion anisotropy that is far from uniaxial symmetry. These parameters are also consistent with the other aspects of the phase boundaries discussed.

In particular, we have calculated the low-T behavior of the boundaries to the paramagnetic phase, starting from the complete model Hamiltonian, and using a spin-wave approach. Earlier theoretical work[4-6] predicts a $T^{3/2}$ dependence for the case of uniaxial symmetry and $\mathbf{H}$ applied along the easy axis. This dependence was demonstrated for $NiCl_2 \cdot 6H_2O$.[1] When lower symmetry is considered (orthorhombic exchange or orthorhombic single-ion anisotropy), the easy-axis boundary changes to a T^2 behavior.[7,8] Also, for the boundaries with $\mathbf{H}$ perpendicular to the easy axis, a T^2 dependence is predicted.[9] Two of the above-mentioned references (Refs. 8 and 9) compare their theoretical results with $NiCl_2 \cdot 4H_2O$ data. In both of them, however, a uniaxial model is assumed. In the present calculations, the three boundaries of the paramagnetic phase show a T^2 dependence. When compared with the experimental data, good agreement is found not only with the predicted T^2 dependence, but also with the coefficients of T^2.

II. EXPERIMENTAL DETAILS

A. Experimental setup

The phase boundaries were determined from differential magnetization (dM/dH) measurements taken

as a function of an applied magnetic field at fixed temperatures below 4K. The ac mutual inductance bridge and the variable temperature cryostat used are described in Ref. 1. The external field was provided by a superconducting Nb_3Sn magnet. The susceptibility data were taken at the fixed frequency of 155 Hz.

B. Samples

Single crystals of $NiCl_2 \cdot 4H_2O$ were grown from slow evaporation of a saturated solution of reagent grade $NiCl_2 \cdot 6H_2O$ maintained in a temperature controlled bath at $50.0 \pm 0.1\,^{\circ}C$. Since the tetrahydrated crystal is isomorphous with $MnCl_2 \cdot 4H_2O$ (Ref. 10) the crystal axes could be identified from the growth habit described by Groth[11] for the latter.

$NiCl_2 \cdot 4H_2O$ exhibits antiferromagnetic order below 3 K.[2] No direct information on its magnetic structure is available but magnetic susceptibility measurements indicate that the easy axis is near the crystallographic c axis. This is the same easy axis found in the isomorphous $MnCl_2 \cdot 4H_2O$. It is thus likely, as pointed out in Ref. 2, that both antiferromagnets have the same magnetic structure. The magnetic structure of the Mn salt is well known.[12] A close look into its structure shows that it can be described approximately in terms of two sublattices, with each magnetic ion being coordinated to six nearest neighbors of opposite spin.

These compounds crystallize in the monoclinic system.[2,13] The four water molecules and the two chloride ions form a distorted octahedron around the magnetic ion. The chloride ions are adjacent to one another in the octahedron. This structure indicates that the distortion of the cubic crystalline field acting on each Ni ion is of low symmetry and an orthorhombic term must be included in the model Hamiltonian.

Rod-shaped samples of $NiCl_2 \cdot 4H_2O$ were cut from single crystals with their axis along the direction in which the external field was applied. Typical dimensions were 7 mm long and 3 mm in diameter. The estimated demagnetization factor was $(N/4\pi) = 0.12$.

III. EXPERIMENTAL RESULTS

A. Phase boundaries

Most of the transition fields were obtained from continuous curves of dM/dH versus H at constant T. Figure 1 shows two of these curves for **H** applied along the easy axis (the crystallographic c axis). For $T = 1.22$ K, the trace shows a huge peak at the spin-flop transition and a lambda-shaped peak at the second-order transition from the spin-flop phase to the paramagnetic phase (SF-P). At temperatures above the bicritical point, a single anomaly is observed which corresponds to the second order transition from the antiferromagnet phase to the paramagnetic phase (AF-P) (see curve for $T = 2.47$ K in Fig. 1).

When **H** is applied along the principal directions perpendicular to the easy axis, the crystallographic axes b and a', dM/dH is found to be almost independent of T and H, until the second-order transition to the paramagnetic phase occurs. This transition is also marked by a lambda-shaped peak. The axis a' is perpendicular to both b and c, and is a few degrees away from the a axis. The assignment of these axes is illustrated in Fig. 2.

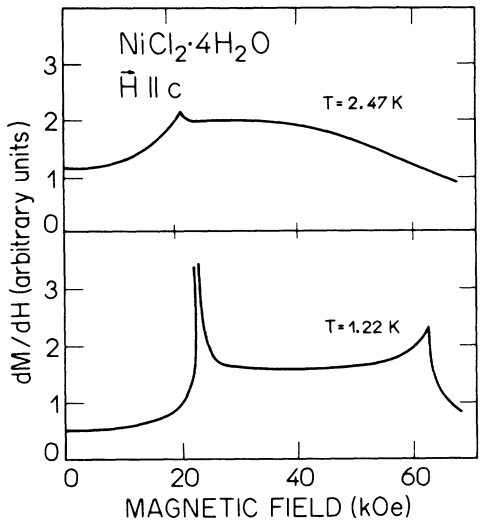

FIG. 1. Two dM/dH traces for **H** along the easy axis. At $T = 1.22$ K the spin-flop transition and the transition from the spin-flop phase to the paramagnetic phase are clear. At $T = 2.47$ K the single transition from the antiferromagnetic phase to the paramagnetic phase appears.

The critical transition fields, for **H** parallel to c, are shown in Fig. 3. In this figure, some of the points near the bicritical point were obtained from curves of dM/dH versus T at constant H. Figure 4 displays the transition fields for **H** along b and a'.

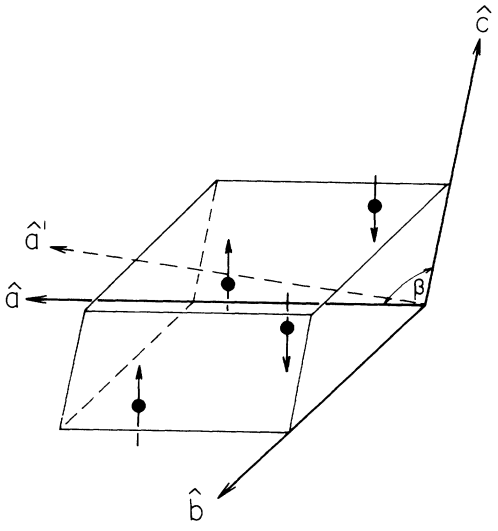

FIG. 2. Magnetic unit cell of $MnCl_2 \cdot 4H_2O$ from Ref. 12. In our work the magnetic field is applied along the axes $\hat{a}$, $\hat{b}$, and $\hat{c}$, with $\hat{a}'$ being perpendicular to $\hat{b}$ and $\hat{c}$ axes. The solid arrows indicate spin directions.

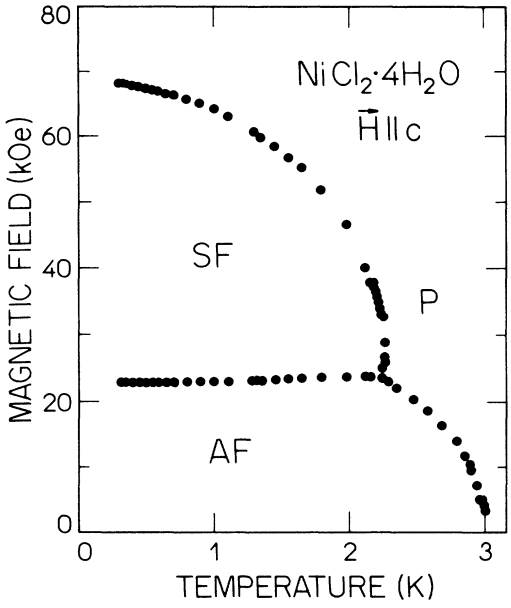

FIG. 3. Magnetic phase diagram for **H** parallel to the c axis. The boundaries separate the antiferromagnet (AF), spin-flop (SF), and the paramagnetic (P) phases.

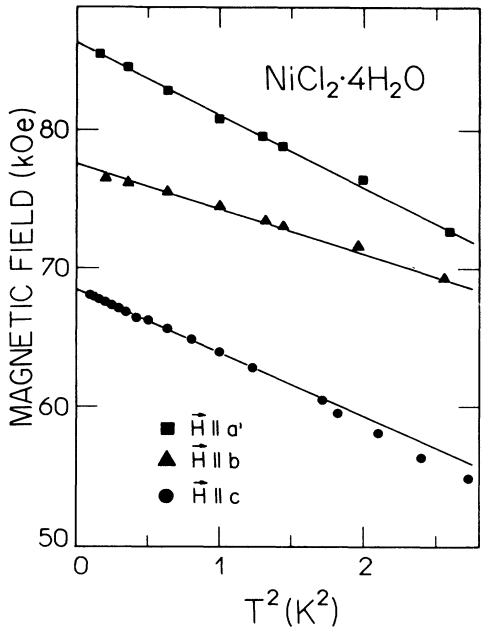

FIG. 5. Low-T boundaries to the paramagnetic phase. The solid lines correspond to the expressions (2), (3), and (4) with the parameters given in Sec. V A.

B. Néel temperature

The ordering temperature at zero field T_N was determined from the extrapolation of the AF-P boundary at low fields. Figure 5 is a plot of these data for **H** parallel to the easy axis. Molecular field theory predicts a H^2 dependence for this boundary,[14] and the extrapolation was done on that basis. We obtained $T_N = 3.00 \pm 0.01$ K, in good agreement with the reported value $T_N = 2.99 \pm 0.01$ K from specific-heat measurements.[2]

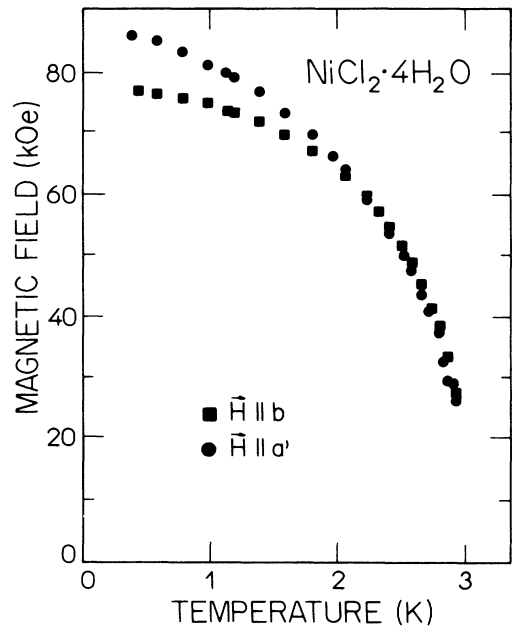

FIG. 4. Magnetic phase diagrams for **H** parallel to b and a'.

C. $T = 0$ transition fields

The $T = 0$ transition fields were obtained from extrapolation of the boundaries. The spin-flop boundary was assumed to be temperature independent at low T, resulting in $H_{SF}(0) = 23.0$ kOe. The boundaries of the paramagnetic phase were extrapolated by a T^2 law, following the theoretical predictions. The results were $H_c(0) = 68.35$ kOe, $H_b(0) = 77.54$ kOe, and $H_{a'}(0) = 86.40$ kOe.

IV. THEORETICAL RESULTS

We considered a two-sublattice (α,β) anisotropic antiferromagnet defined by a spin Hamiltonian of the form

$$H = \sum_{\alpha,\beta} [J(S_\alpha^x S_\beta^x + S_\alpha^y S_\beta^y) + J^z S_\alpha^z S_\beta^z] + L \sum_\alpha (S_\alpha^z)^2 + E \sum_\alpha [(S_\alpha^x)^2 - (S_\alpha^y)^2] - g\mu_B \mathbf{H} \cdot \sum_\alpha \mathbf{S}_\alpha , \quad (1)$$

where z is the easy axis, y is the intermediate axis, and x is the hard axis. J and J^z are the exchange parameters, and L and E are the single-ion uniaxial and orthorhombic anisotropy parameters, respectively. The other symbols have their usual meanings. The sum (α,β) runs over all nearest-neighbor pairs. To obtain the magnetic boundaries to the paramagnetic phase at low temperatures we used the Green's function method. Some details of the calculations are explained in the Appendix. We stress here that we considered only terms to order $1/S$,[15] and two magnetic ions per sublattice and per unit cell.

When **H** is applied along z, the T dependence of the

SF-P transition field is given by

$$g\mu_B H_c^z(T)=nS(J+J^z)+2S(L+E)$$
$$-\frac{3\xi}{8\pi^2}\frac{3(J+J^z)+L+E}{E^{1/2}J^{3/2}}\left[\frac{k_BT}{S}\right]^2, \quad (2)$$

where the condition $E>0$ was used. Here, n is the number of nearest neighbors of a given magnetic ion, k_B is the Boltzman factor, and $\xi(2)=\sum_{r=1}^{\infty}(1/r^2)$.

For **H** applied along y, the low-T boundary is

$$g\mu_B H_c^y(T)=nS(J+J^z)-2S(L+E)$$
$$-\frac{3\xi(2)}{4\pi^2\sqrt{2}}\frac{3(J+J^z)-(L+E)}{[3(J^z-J)-(L-E)]^{1/2}}$$
$$\times\frac{1}{(J^z)^{3/2}}\left[\frac{k_BT}{S}\right]^2, \quad (3)$$

where the condition $nS(J^z-J)>2S(L-E)$ is satisfied.

For **H** parallel to x, the corresponding result is

$$g\mu_B H_c^x(T)=nS(J+J^z)-2S(L-E)$$
$$-\frac{3\xi(2)}{4\pi^2\sqrt{2}}\frac{3(J^z+J)-(L-E)}{[3(J^z-J)-(L+E)]^{1/2}}$$
$$\times\frac{1}{(J^z)^{3/2}}\left[\frac{k_BT}{S}\right]^2, \quad (4)$$

where the conditions for the existence of this solution are $nS(J^z-J)>2S(L+E)$, $J^z>J$, $L<0$, and $E>0$.

The first-order transition field between the antiferromagnetic and the spin-flop phases was obtained by equating the free energies of these two phases. The result at $T=0$ is

$$g\mu_B H_{SF}(0)=S[n(J^z-J)-2(L+E)]^{1/2}$$
$$\times[n(J+J^z)+2(L+E)]^{1/2} \quad (5)$$

with the condition $n(J^z-J)>2(L+E)$.

It is worth noting that the above expressions for the critical fields agree with the molecular field theory (MFT) predictions at $T=0$. This can be seen, for instance, by comparing the present expressions at $T=0$ with the ones given by Gorter and Van Peski-Tinbergen[16] (for this comparison one shall make the following substitutions in their expressions: $A_x=A_y=nJ$; $A_z=nJ^z$; $D_z=-2L$; $D_n=-Dy=2E$). Earlier calculations for the perpendicular direction do not show this agreement. The difference is the particular choice of spin operators, as described in the Appendix.

V. DISCUSSION AND CONCLUSIONS

A. Exchange and anisotropy parameters

From the experimental values of the $T=0$ transition fields and the theoretical expressions (2)–(5) we calculated the crystal-field parameters. Using a g factor of 2.28 (as obtained in Ref. 2), $S=1$ and $n=6$ we found $J^z/k_B=0.971$ K, $J/k_B=0.891$ K, $L/k_B=-0.691$ K, and $E/k_B=0.339$ K. The negative sign of L indicates that the single-ion states $(1/\sqrt{2})(|1\rangle\pm|-1\rangle)$ have energies which are lower than the energy of the singlet $|0\rangle$ by the amounts $L\pm E$. The relative values of these parameters show that the symmetry of the crystalline field on the Ni^{2+} is far from uniaxial, the highest anisotropy being in the $a'b$ plane. On the other hand, the relative values of J^z and J, $(J/J^z)\simeq 0.9$, indicate that the exchange interaction is not strongly anisotropic.

B. Low-temperature paramagnetic boundaries

The low-temperature dependence of the SF-P boundary for **H** parallel to the easy axis is extensively discussed in Ref. 1. There, a detailed analysis of the experimental data for $NiCl_2\cdot 6H_2O$ is presented demonstrating the $T^{3/2}$ dependence predicted for uniaxial symmetry. In $NiCl_2\cdot 6H_2O$, as well as in $NiCl_2\cdot 4H_2O$, the crystalline field is produced mainly by an octahedron that surrounds the Ni ion and which is composed by four electrically polarized H_2O molecules and the two Cl ions. In $NiCl_2\cdot 6H_2O$ the Cl ions occupy opposite vertices of the octahedron (*trans*position)[17] and the anisotropy is mostly uniaxial. In $NiCl_2\cdot 4H_2O$, however, the Cl ions occupy adjacent vertices of the octahedron (*cis*position), and consequently a large orthorhombic component is expected.[2] For this reason we have included anisotropic exchange and orthorhombic parameters in our model Hamiltonian.

The calculations of the low-T boundaries described in the Appendix result in a T^2 dependence for **H** parallel and perpendicular to the easy axis [Eqs. (2)–(4)]. They differ from earlier published calculations in two aspects. First, the starting Hamiltonian includes both anisotropic exchange and orthorhombic single-ion anisotropy. Second, the present calculations lead to $T=0$ transition fields which agree with MFT.

Figure 5 shows the experimental data for all the three phase boundaries in an H versus T^2 plot. The solid lines represent the theoretical expressions (2), (3), and (4), which correspond, respectively, to the axes c, b, and a', and which were obtained using the parameters described in the preceding section. It is clear that the data are consistent not only with the predicted asymptotic T^2 dependence, but also with the predicted coefficient of the T^2. The calculated values of these coefficients are 4.365 kOe/K^2 for the c axis, 3.179 kOe/K^2 for the b axis, and 5.185 kOe/K^2 for the a' axis. The agreement between the data and the present calculations is good. It is interesting to note that the slope for the intermediate axis is smaller than that of the other two. It is interesting to point out also, that the solid lines in Fig. 5 describe the data for the for the hard and intermediate axes, actually until beyond the plotted temperatures (>1.6 K), although for the easy axis the experimental points start to deviate right above 1.2 K. This is due, probably, to the presence of the bicritical point at $T_b=2.22$ K. This special critical point governs the behavior of the boundaries in its vicinity, as will be discussed later.

C. Néel temperature

A review of the predictions of the high-temperature series (HTS) expansions for the critical temperatures of

isotropic ferromagnets and and antiferromagnets was done by Rushbrooke *et al.*[18] For general spin values the available estimates are those of Rushbrooke and Wood[19] based on the analysis of the HTS for the Heisenberg model. For a ferromagnet with a given $|J|$ they propose that

$$T_c = \frac{n-1}{2}\frac{|J|}{k_B}[0.579S(S+1)-0.072] \tag{6}$$

and for antiferromagnets with the same $|J|$, T_N can be estimated according to

$$T_N = \left[1+\frac{0.65}{nS(S+1)}\right]T_c \tag{7}$$

with T_c given by (6). These expressions are claimed to be accurate within few percent. In fact a latter estimate of Ritchie and Fisher[20] for $S=1$ based on HTS give a value 4% smaller than that calculated from (6).

Using our experimentally derived value of J in the above expressions we get $T_N = 2.55$ K, a value well below the one observed experimentally. These expressions, however, apply to isotropic systems, and we still have to account for the effect of the anisotropic exchange and crystal-field anisotropy.

The influence of the ratio J/J^z has been studied from high-temperature series expansions by Jou and Chen[21] for $S=\frac{1}{2}$ and by Mouritsen *et al.*[22] for a classical spin ($S\to\infty$). For a ratio of 0.9 (present case) the estimated corrections are $+6.3\%$ for $S=\frac{1}{2}$ and $+3.4\%$ for $S\to\infty$. These corrections bring our theoretical T_N (for $S=1$) to a value between 2.62 and 2.7 K. The influence of the crystal-field anisotropy was discussed by Lines[23] and Devlin[24] in the MF and also using various decoupling procedures for the Green's function method. Brankov *et al.*,[25] from high-temperature series expansions, conclude that the MFT results work better. Considering an experimental ratio $(L/J)=0.77$, and the curves for a magnetic simple-cubic lattice of Ref. 23, the estimated correction factor is 1.07. This brings the theoretical prediction to between 2.8 and 2.9 K, a value already close to the experimental one. We do not know of any work that includes the influence of E on T_N.

D. The easy-axis AF-P boundary near T_N

In Fig. 6, the AF-P boundary for **H** parallel to the easy axis is plotted against H^2. The data suggest an asymptotic quadratic dependence, which, in fact, is predicted by high-temperature series expansion.[22] In this reference the authors also conclude that the exchange anisotropy should not affect the slope of the H^2. In the MFT the entire boundary is quadratic[14,26] and Shapira and Foner[26] give the following expression for its slope:

$$\frac{T_N - T_C(H)}{H^2} = \frac{2S^2+2S+1}{40k_B^2 T_N}g^2\mu_B^2 \ . \tag{8}$$

Shapira[27] also estimated the influence of the crystal-field parameter on the boundary, to first order in L/k_BT. For $S=1$ the single-ion anisotropy has no effect on the slope.

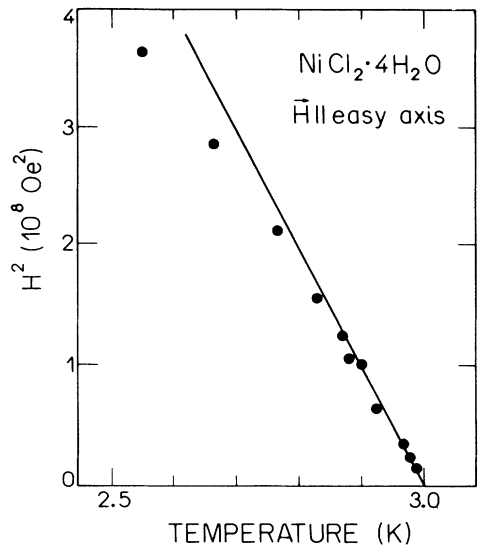

FIG. 6. Antiferromagnetic-paramagnetic boundary near T_N. The solid lines correspond to the Eq. (8).

Expression (8) yields the value 9.75×10^{-10} K/Oe^2 which was used to generate the solid line in Fig. 6. The agreement at low fields is quite good.

E. The bicritical point (BP)

The extended scaling theory predicts that the AF-P and the SF-P critical lines meet the SF line tangentially at the bicritical point (H_b, T_b).[28,29] The mathematical expressions for these phase boundaries near the BP and the choice of the best scaling axes are discussed in Ref. 30. For our discussion, the relevant point is that our compound should be a representative of an $N=2$ system (N being the spin dimensionality at the BP). This is due to the orthorhombic character of the anisotropy, which causes both critical lines approaching the BP to have an Ising-like behavior. A uniaxial anisotropy would correspond to $N=3$.

Figure 7 compares our data with fits to the theoretical predictions for the $N=3$ case (solid line) and $N=2$ (dashed line). The theoretical curves were obtained by least-squares fits of the data to the equations $\tilde{g}=\omega_\perp \tilde{t}^{\,\phi}$ for the SF-P boundary and $\tilde{g}=-\omega_\parallel \tilde{t}^{\,\phi}$ for the AF-P boundary. Here, $\tilde{g}=g-pt$ and $\tilde{t}=t+qg$, where $g=H^2-H_b^2$ and $t=(T-T_b)/T_b$. The parameter $p=(1/T_b)(dH_{SF}^2/dT)_b$ was obtained from the tangent to the experimental spin-flop boundary at $T_b=2.22$ K, resulting in $p=41.2$ kOe^2/K^2. The parameter

$$q=[(N+2)/3NT_b](dT_c/dH^2)_{H=0}$$

was determined from the experimental slope of the easy-axis AF-P boundary near T_N, resulting in $q=2.68\times10^{-4}$ kOe^{-2} for $N=3$, and $q=3.21$ kOe^{-4} for $N=2$. The crossover exponent ϕ and the amplitude ratio $\omega_\perp/\omega_\parallel$ were taken at their theoretically predicted values[31] $\phi=1.25$

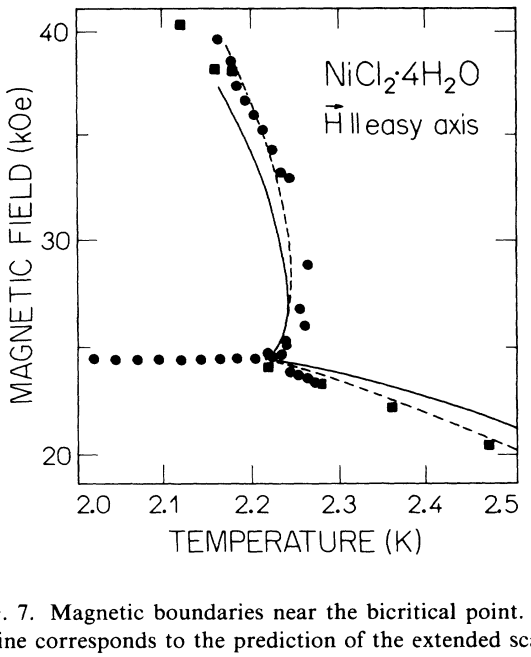

FIG. 7. Magnetic boundaries near the bicritical point. The solid line corresponds to the prediction of the extended scaling theory for $N=3$, and the dashed line for $N=2$.

and $(\omega_\perp/\omega_\parallel)=2.51$ for $N=3$ and $\phi=1.175$ and $\omega_\perp=\omega_\parallel$ for $N=2$. Therefore, the only adjustable parameter was one of the amplitudes ω. Clearly, the data points are much better described by the $N=2$ curve.

ACKNOWLEDGMENTS

We are grateful to S. R. Salinas for useful discussions. The Instituto de Física da Universidade de Sao Paulo is supported by Financiadora de Estudos e Projetos (FINEP), Fundaçaño de Amparoe Pesquisa do Estado de Saño Paulo (FAPESP), and Conselho Nacional de Desenvolvimento Cimento Científico e Tecnologico (CNPq) (Brazil).

APPENDIX

To obtain the temperature dependence of the phase boundaries of the paramagnetic phase at low temperatures from the spin Hamiltonian (1), we introduce raising and lowering spin operators S^+ and S^- for each one of the directions in which the field is applied. For the sublattice we write

$S_\alpha^\pm = S_\alpha^z \pm iS_\alpha^y$ for **H** parallel to z (easy axis) ,

$S_\alpha^\pm = S_\alpha^z \pm iS_\alpha^x$ for **H** parallel to y (intermediate axis) ,

and

$S_\alpha^\pm = S_\alpha^z \pm iS_\alpha^y$ for **H** parallel to x (hard axis) .

These definitions preserve the commutation rules for the spin operators. For instance, for **H** along the z direction these rules are

$$[S_\alpha^+, S_\alpha^-]=2S_\alpha^z, \quad [S_\alpha^z, S_\alpha^-]=-S_\alpha^- ,$$

and

$$[S_\alpha^z, S_\alpha^+]=S_\alpha^+ .$$

When **H** is applied along x and y, S_α^z must be replaced, respectively, by S_α^x and S_α^y.

For **H** parallel to x, we observe that the present choice of S^+ and S^- is different from that used in Refs. 7 and 9. Although that choice also preserves the commutation rules, the present one leads to $T=0$ transition fields that agree with MFT for **H** perpendicular to z.

Next we introduce the Holstein-Primakoff transformation:

$$S_\alpha^+ = (2S)^{1/2} f_\alpha(S) a_\alpha ,$$

$$S_\alpha^- = (2S) a_\alpha^\dagger f_\alpha(S) ,$$

$$S_\alpha^i = S - a_\alpha^\dagger a_\alpha ,$$

where

$$f_\alpha(S)=[1-(a_\alpha^\dagger a_\alpha/2S)]^{1/2}$$

and $i=(x,y,z)$.

At low temperatures it is reasonable to consider the approximation

$$f_\alpha(S) \simeq 1-(1/4S) a_\alpha^\dagger a_\alpha .$$

If we now introduce the lattice Fourier transformation we obtain a Hamiltonian that contains products of two and four spin-wave operators up to the order $1/S$. Next we write the equation of motion for the Green's function $\langle\langle a_{\mathbf{k}}; a_{k'}^\dagger \rangle\rangle$ and $\langle\langle a_{-\mathbf{k}}^\dagger; a_{k'}^\dagger \rangle\rangle$ where $\mathbf{k}$ is the reciprocal-lattice vector belonging to the first Brillouin zone of the simple-cubic lattice. Within the random phase approximation we obtain a renormalized magnon energy spectrum $\varepsilon_{\mathbf{k}}(T,H)$. The critical fields are determined from $\varepsilon_{\mathbf{k}_v}(T,H)=0$, where $\mathbf{k}_v$ is a vector that points to the corner of the Brillouin zone. Neglecting the small zero-point corrections, and noting that, near the corners of the Brillouin zone, $\varepsilon_{\mathbf{k}} \simeq A\,|\,\mathbf{k}-\mathbf{k}_v\,|$ where A is a constant, we obtain the dominant term in the temperature. The results are the three equations (2), (3), and (4).

[1]N. F. Oliveira, Jr., A. Paduan-Filho, S. R. Salinas, and C. C. Becerra, Phys. Rev. B **18**, 6165 (1978).

[2]J. N. McElearny, D. B. Losee, S. Merchant, and R. L. Carlin, Phys. Rev. B 7, 3314 (1973).

[3]A. Paduan-Filho, C. C. Becerra, and N. F. Oliveira, Jr., Phys. Lett. **50A**, 51 (1974).

[4]H. Falk, Phys. Rev. **133**, A1382 (1964).

[5]F. B. Anderson and H. B. Callen, Phys. Rev. **136**, A1068 (1964).

[6]J. Feder and E. Pytte, Phys. Rev. **168**, 640 (1968).

[7]M. Cieplak, Phys. Rev. B **15**, 5310 (1977).
[8]W. Figueiredo and S. R. Salinas, Physica **124B**, 259 (1984).
[9]W. Figueiredo, S. R. Salinas, C. C. Becerra, N. F. Oliveira, Jr., and A. Paduan-Filho, J. Phys. C **15**, L115 (1982).
[10]A. Nenhans, Chem. Erde **5**, 554 (1930).
[11]P. Groth, *Chemishe Kristallographie* (Wilhelm Engleman, Leipzig, 1908), Vol. I.
[12]R. F. Altman, S. Spooner, D. P. Landau, and J. E. Rives, Phys. Rev. B **11**, 458 (1975).
[13]A. Zalkin, J. D. Forrester, and D. H. Templeton, Inorg. Chem. **3**, 529 (1964); Z. M. El Saffar and G. M. Brown, Acta Crystallogr. B **27**, 66 (1971).
[14]P. Heller, Phys. Rev. **146**, 403 (1966).
[15]For the meaning of the leading order in $1/S$ we refer to the discussion at the bottom of p. 645 of Ref. 6.
[16]C. J. Gorter and Van Peski-Tinbergen, Physica **22**, 273 (1956).
[17]J. Mizuno, J. Phys. Soc. Jpn. **16**, 1574 (1961).
[18]G. S. Rushbrooke, G. A. Baker, and P. J. Wood, in *Phase Transitions and Critical Phenomena,* edited by C. Domb and M. S. Green (Academic, New York, 1974), Vol. III, pp. 306–307.
[19]G. S. Rushbrooke and P. J. Wood, Mol. Phys. **6**, 409 (1963).
[20]D. S. Ritchie and M. E. Fisher, Phys. Rev. B **5**, 2668 (1972).
[21]D. C. Jou and H. H. Chen, Phys. Lett. **45A**, 239 (1973).
[22]O. G. Mouritsen, E. Kjaersgard, and S. J. Knak Jensen, Phys. Rev. B **22**, 3256 (1980).
[23]M. E. Lines, Phys. Rev. **156**, 534 (1967).
[24]J. F. Devlin, Phys. Rev. B **4**, 136 (1971).
[25]J. G. Brankov, J. Przystawa, and E. Praveczki, J. Phys. C **5**, 3387 (1972).
[26]Y. Shapira and S. Foner, Phys. Rev. B **1**, 3083 (1970).
[27]Y. Shapira, Phys. Rev. B **2**, 2725 (1970).
[28]M. E. Fisher and D. R. Nelson, Phys. Rev. Lett. **32**, 1550 (1974).
[29]J. M. Kosterlitz, D. R. Nelson, and M. E. Fisher, Phys. Rev. B **13**, 412 (1976).
[30]M. E. Fisher, Phys. Rev. Lett. **34**, 1634 (1975).
[31]P. Pfeuty, D. Jasnow, and M. E. Fisher, Phys. Rev. B **10**, 2088 (1974).